Comprehensive Optimization of Optical Efficiency and Thermal Power Output in Tower Solar Thermal Power Stations

Rende Chen, Xiaozhou Zhou, Hongwei Song *

School of Automotive and Traffic Engineering, Jiangsu University, Zhenjiang, China, 212013

* Corresponding Author Email: songhw0501@163.com

Abstract. Recent years have seen a rise in interest in renewable energy sources, particularly efficient, sustainable, and ecologically friendly solar thermal power generation, due to rising worldwide energy demand and environmental consciousness. The effectiveness of a tower-type photovoltaic power-generating system, which uses concentrated solar radiation to create electricity, is greatly dependent on the design and functionality of its heliostat mirrors. This work develops a single-objective optimization model to optimize the yearly average thermal power production per unit mirror area based on a fixed-sun mirror field model of a tower-type solar thermal power plant. This study uses the approximate formulas for the solar declination angle and solar time angle proposed by Cooper to determine the sun's position at that time. The HFLCAL model has been developed to establish an optical efficiency model for the heliostat field, utilizing the Campo arrangement method to produce a densely packed heliostat field. Finally, a genetic algorithm is employed to determine the optimal unit of mirror surface area, which is calculated to be 0.9575*MW*. The absorption tower is located at (0,-87.5656). The heliostat measures 4.7825*m*×4.3666*m* (width×height), with an installation height of 3.1332*m*, and there are a total of 3010 heliostats.

Keywords: Transformation of the energy matrix, Campo setup, genetic algorithm.

1. Introduction

In recent years, the increasing global demand for energy and the escalating significance of environmental conservation have prompted a surge in interest in the development and utilization of renewable energy across the international community. Tower-type solar thermal power generation, among numerous renewable energy technologies, has garnered widespread attention for its high efficiency, sustainability, and environmentally friendly features. This system generates thermal energy by concentrating solar energy, which is subsequently converted into electrical energy. Within this process, the configuration and performance of the heliostat significantly determine the system's efficiency, emphasizing the pivotal role of heliostat technology in advancing solar thermal power generation.

This paper assumes that all heliostats in the heliostat field are of uniform size and installation height. The heliostat field parameters, including the position coordinates of the absorption tower, the dimensions of the heliostat mirrors, the mounting height, the quantity of mirrors, and the fixed-sun mirror position, have been carefully designed in accordance with exact specifications.These design parameters are optimized to achieve an annual average thermal power output of 60*MV* for the fixed-sun mirror field while maximizing the annual average thermal power output per unit mirror area.

This paper details a methodical approach for optimizing a heliostat field for solar energy generation. It begins with modeling the sun's position using Cooper's formula for solar declination and solar hour angle, tailored to local latitude. This establishes a coordinate system based on light reflection principles for the field. The paper then develops an optical efficiency model employing ray-tracing, flat projection, and the HFLCAL model, alongside a thermal power model derived from the Direct Normal Irradiance formula. The study is centered on two single-objective optimization models, both utilizing the Campo arrangement for a heliostat field. The first model aims to maximize the annual average thermal power output per mirror unit for a densely packed heliostat field. On the other hand, the second model focuses on optimizing the annual average power output for a fixed-sun mirror field, also employing the Campo method. Both models are resolved using a genetic algorithm, illustrating a comprehensive strategy for enhancing solar energy efficiency through advanced heliostat field design.

2. Study on Optical Characteristics of Heliostat Field

2.1. Preparing to model a fixed mirror solar field

The implementation of the fixed-heaven mirror field model is preceded by establishing the Earth coordinate system and the fixed-heaven mirror coordinate system. This system is also referred to as the mirror field coordinate system or the Earth coordinate system. As shown in Figure 1.

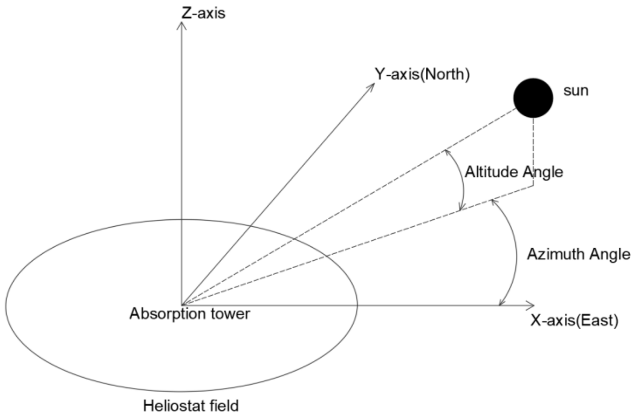

Figure 1 Earth coordinate system (mirror field coordinate system)

Establishing a coordinate system on each heliostat involves analyzing key factors such as the heliostat surface normal, incident light, angle of incidence, surface normal vector, reflected light, and angle of reflection. This systematic approach is crucial for accurately analyzing and calculating the reflective properties of the heliostat.

2.2. Modeling of the fixed-heaven mirror field

2.2.1 Solar position (altitude angle αS, azimuth γS, solar time angle ω, angle of azimuth δ)

The calculation formula for solar altitude angle α_S[1]:

$$\sin\alpha_S = \cos\delta\cos\varphi\cos\omega + \sin\delta\sin\varphi \tag{1}$$

Calculation formula for solar azimuth γ_S[1]:

$$\cos\gamma_S = \frac{\sin\delta - \sin\alpha_S\sin\varphi}{\cos\alpha_S\cos\varphi} \tag{2}$$

The solar time angle ω is calculated as:

$$\omega = \frac{\pi}{12}(ST - 12) \tag{3}$$

where ST is the local time.

The solar declination angle δ is calculated using Cooper's 1969 approximate formula [2]:

$$\delta = 23.45\sin(2\pi\frac{284 + D}{365}) \tag{4}$$

where D is the yearly accumulation of days:

$$D = floor(month \times 275/9) - floor\left((month+9)/12\right) \times \left(floor\left(\left(year - 4 \times floor\left(year/4\right)+2\right)/3\right)+1\right) + day - 30 \tag{5}$$

2.2.2 Normal radiant irradiance *DNI*

The standard radiant irradiance *DNI* is calculated using this equation [3]:

$$\begin{cases} DNI = G_0\left[a + b\exp\left(-\dfrac{c}{\sin\alpha_S}\right)\right] \\ a = 0.4237 - 0.00821(6-H)^2 \\ b = 0.5055 + 0.00595(6.5-H)^2 \\ c = 0.2711 + 0.01858(2.5-H)^2 \end{cases} \tag{6}$$

where G_0 is the solar constant, $G_0 = 1.366\ kW/m^2$; H is the altitude, $H = 3\ km$.

2.2.3 Heliostat optical efficiency *η*

Each heliostat's efficiency is denoted as η_i, and the overall efficiency η is calculated as follows:

$$\eta = \eta_{sb}\eta_{\cos}\eta_{at}\eta_{trunc}\eta_{ref} \tag{7}$$

2.2.4 The thermal power output of the heliostat field is denoted as E_{field}

The output thermal power E_{field} of the fixed-sky mirror field is given by:

$$E_{field} = DNI\square\sum_{i}^{N} A\eta_{sb}\eta_i \tag{8}$$

2.3. Fixed-heaven mirror field model solution

Step1. Initial conditions

$$\begin{cases} x_0 = 0, y_0 = 0, z_0 = 80 + \dfrac{1}{2}\times 8 = 84, z_i = 4 \\ \varphi = 39.4°, ST = 9,10.5,12,13.5,15 \\ G_0 = 1.366, H = 3, N = 1745, LW = 6, LH = 6 \\ N = 1745, \eta_{ref} = 0.92 \end{cases} \tag{9}$$

Step2. Model Solving

2.3.1 Determine the vector using the sun's position

Each local time in *ST* corresponds to different *j* values, and for each of these times, the 21st day of the 12th month is taken as the annual cumulative day, giving rise to *k* ($j = 5$, $k = 12$) different annual cumulative days. As a result, the sun's altitude angle and azimuth angle vary for each of these different times, which in turn affects the incident light unit vector and other related quantities.

The analysis of the model solution is considered only for a certain time case, a certain date mirror, satisfying Eq:

$$\begin{cases} \sin\alpha_S = \cos\delta\cos\varphi\cos\omega + \sin\delta\sin\varphi \\ \cos\gamma_S = \dfrac{\sin\delta - \sin\alpha_S\sin\varphi}{\cos\alpha_S\cos\varphi} \\ \omega = \dfrac{\pi}{12}(ST-12) \\ \delta = 23.45\sin(2\pi\dfrac{284+D}{365}) \end{cases} \tag{10}$$

The above calculations to get a certain time in the case of the sun's altitude angle and azimuth, are based on the simplification of the sun's conical ray, incident light, and reflected light as a straight-line conical ray of the central axis of the light. After analyzing and processing the incident light unit vector as $\boldsymbol{n_r}=(x_r,y_r,z_r)$, it passes through the center of a heliostat:

$$\begin{cases} x_r = \cos\alpha_S\cos(\gamma_S - 90°) \\ y_r = \cos\alpha_S\sin(\gamma_S - 90°) \\ z_r = \sin\alpha_S \end{cases} \tag{11}$$

The heliostat directs light towards the center of the collector, using the unit vector $\boldsymbol{n_f}=(x_f,y_f,z_f)$ to represent the reflected light direction after analysis and processing:

$$\overrightarrow{n_f} = \frac{P_0 - P}{|P_0 - P|} = \frac{(-x_i, -y_i, z_0 - z_i)}{\sqrt{x_i^2 + y_i^2 + (z_0 - z_i)^2}} \tag{12}$$

The normal vector of the fixed-sun mirror is determined by analyzing the unit vectors of the incident and reflected light, as expressed by:

$$\vec{n} = \frac{\overrightarrow{n_f} - \overrightarrow{n_r}}{\left|\overrightarrow{n_f} - \overrightarrow{n_r}\right|} \tag{13}$$

Determine the pitch angle θ_1 and azimuth angle θ_2 of the heliostat using vectors:

$$\begin{cases} \tan\theta_1 = \dfrac{z_i + \sin\alpha_s \cdot m}{\sqrt{x_i^2 + y_i^2 + (x_i^2 + y_i^2 + z_i^2)\cos^2\alpha_S - 2\cos\alpha_S \cdot (x_i\sin\gamma_s - y_i\cos\alpha_i) \cdot m}} \\ \tan\theta_2 = \dfrac{x_i - \cos\alpha_s\sin\gamma_s \cdot m}{\sqrt{x_i^2 + y_i^2 + (x_i^2 + y_i^2 + z_i^2)\cos^2\alpha_S - 2\cos\alpha_S \cdot (x_i\sin\gamma_s - y_i\cos\alpha_i) \cdot m}} \end{cases} \tag{14}$$

where $m=(x_i^2+y_i^2+z_i^2)^{1/2}$.

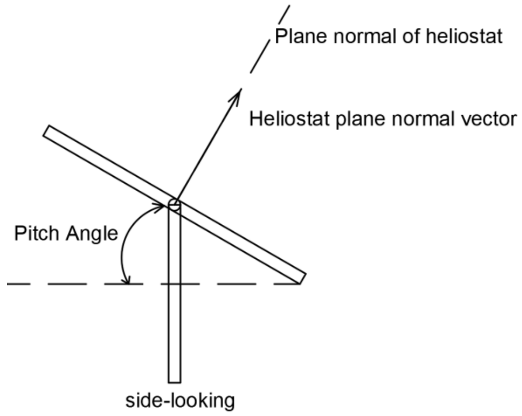

Figure 2 Diagram of azimuthal angle

2.3.2 Solve for the cosine efficiency η_{cos}

The analysis of the heliostat coordinate system begins by defining any heliostat as heliostat *A*. The coordinate system consists of three axes: x_A, y_A, and z_A, with the corresponding angles of incidence and reflection as shown in Figure 2. The angles between the angle of incidence and the angle of reflection, as well as the angle normal to the heliostat, are all denoted as θ [4].

$$\begin{cases} \eta_{\cos} = \cos\theta = \vec{n} \cdot \vec{i} \\ \vec{i} = (-\cos\alpha_S \sin\gamma_S, -\cos\alpha_S \cos\gamma_S, -\sin\alpha_S) \end{cases} \tag{15}$$

2.3.3 Determine the atmospheric transmittance, denoted as η_{at}

The distance, d_{HR}, between the heliostat center and the collector center can be calculated using the Earth's coordinate system.When d_{HR} is 1000 or less, the atmospheric transmittance is determined[5]:

$$\begin{cases} \eta_{at} = 0.99321 - 0.0001176 d_{HR} + 1.97\times10^{-8}\times d_{HR}^2 \\ d_{HR} = \sqrt{(x_i - x_0)^2 + (y_i - y_0)^2 + (z_i - z_0)^2} \end{cases} \tag{16}$$

2.3.4 Calculate the value of specular reflectance η_{ref}

The reflectance, represented by η_{ref}, is a constant at 0.92.

2.3.5 Solve for the shadowing occlusion efficiency η_{sb}

The idea below can be utilized to calculate shadow shading efficiency[6]:

$$\eta_{sb} = 1 - \frac{\text{Shadow and mirror masking area}}{\text{Mirror area}} \tag{17}$$

Consideration is given to both the fixed-sun mirror coordinate system and the earth coordinate system in the computational framework. To accurately determine the relationship between the mirror coordinate system and the earth coordinate system, the establishment of the unit matrix *T*, representing the transformation, is crucial.

$$T = \begin{pmatrix} \cos(-\theta_2) & -\cos\theta_1 \sin(-\theta_2) & \sin\theta_1 \sin(-\theta_2) \\ \sin(-\theta_2) & \cos\theta_1 \cos(-\theta_2) & -\sin\theta_1 \cos(-\theta_2) \\ 0 & \sin\theta_1 & \cos\theta_1 \end{pmatrix} \tag{18}$$

For further analysis, nine heliostats were selected as a group to make a shadow obscuration schematic as shown in Figure 3:

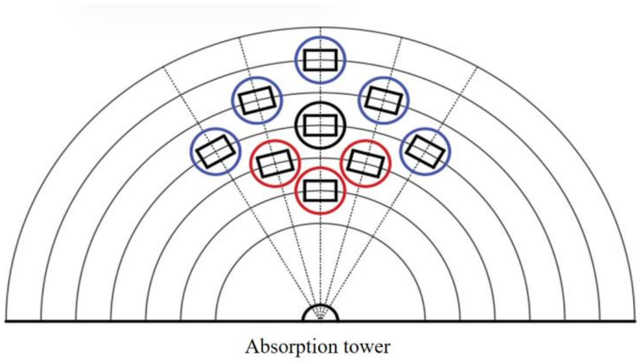

Figure 3 Schematic diagram of shadow masking

The analyzed reference heliostat in the shadow-blocking schematic diagram is the black circle heliostat. The red circle heliostat is responsible for casting "shadow" and "blocking" on the reference heliostat. The combination of the four heliostats in the diagram can be used to analyze the situation of the other heliostats. Similarly, the black circle heliostat participates in influencing the "shadows" and "blocking" of the three blue circle heliostats on the outer side. Moreover, the left and right ends of the red circle heliostat cause "shadows" and "blocking" to the corresponding ends of the blue circle heliostat. This comprehensive analysis provides insights into the impact of different heliostats on each other's "shadow" and "blocking" effects.

Heliostat *A*'s center serves as the origin of the coordinate system labeled O_A, while heliostat *B*'s center functions as the origin of the coordinate system designated as O_B.

The computational solution procedure is as follows:

Setting the step size meshes the heliostat *A* to obtain a shadow masking efficiency of:

$$\eta_{sb} = 1 - \frac{\text{Number of points lost to shadow masking}}{\text{Tropic of Cancer Point A}} \tag{19}$$

Transferring the coordinates $Q_1(x_1,y_1,0)$ of the fixed-heaven mirror *A* to the ground coordinate system yields $Q_1'(x_1',y_1',z_1')$:

$$Q_1' = O_A + T \cdot Q_1 \tag{20}$$

$$Q_1' = O_A + \begin{pmatrix} \cos(-\theta_2) & -\cos\theta_1 \sin(-\theta_2) & \sin\theta_1 \sin(-\theta_2) \\ \sin(-\theta_2) & \cos\theta_1 \cos(-\theta_2) & -\sin\theta_1 \cos(-\theta_2) \\ 0 & \sin\theta_1 & \cos\theta_1 \end{pmatrix} \cdot Q_1 = \begin{pmatrix} x_1' \\ y_1' \\ z_1' \end{pmatrix} \tag{21}$$

Convert Q_1' to Q_1'' to get the heliograph *B* coordinate coordinates, which can be obtained after processing:

$$Q_1'' = \begin{pmatrix} \cos(-\theta_2) & -\cos\theta_1 \sin(-\theta_2) & \sin\theta_1 \sin(-\theta_2) \\ \sin(-\theta_2) & \cos\theta_1 \cos(-\theta_2) & -\sin\theta_1 \cos(-\theta_2) \\ 0 & \sin\theta_1 & \cos\theta_1 \end{pmatrix} \cdot \left(Q_1' - O_B\right) = \begin{pmatrix} x_1'' \\ y_1'' \\ z_1'' \end{pmatrix} \tag{22}$$

At this time, the sunlight incident line is $\boldsymbol{n_r}$, which is transferred from the ground coordinate system to the heliostat *B* coordinate system to obtain $\boldsymbol{N_r}$:

$$\overrightarrow{N_r} = \begin{pmatrix} \cos(-\theta_2) & -\cos\theta_1 \sin(-\theta_2) & \sin\theta_1 \sin(-\theta_2) \\ \sin(-\theta_2) & \cos\theta_1 \cos(-\theta_2) & -\sin\theta_1 \cos(-\theta_2) \\ 0 & \sin\theta_1 & \cos\theta_1 \end{pmatrix}^T \cdot \overrightarrow{n_r} = (a,b,c) \tag{23}$$

Analytically, a relationship between Q_1'' and $Q_2(x_2,y_2,0)$ can be obtained:

$$\begin{cases} x_2 = \dfrac{cx_1 - az_1}{c} \\ y_2 = \dfrac{cy_1 - bz_1}{c} \end{cases} \tag{24}$$

This relation is used to determine whether Q_2 is within the range of the heliostat *B*. The judgmental analysis ultimately yields the shadow shading efficiency η_{sb}.

2.3.6 Solve for the collector truncation efficiency η_{trunc}

The HFLCAL model is used to calculate the collector truncation efficiency, which determines η_{trunc}[7] and is then used to derive the formula:

$$\eta_{trunc} = \frac{1}{2\pi\sigma_{tot}^2} \int_x \int_y \exp\left(-\frac{x^2 + y^2}{\sigma_{tot}^2}\right) dydx \tag{25}$$

$$\begin{cases} \sigma_{tot} = \sqrt{d_{HR}\left(\sigma_{sun}^2 + \sigma_{bq}^2 + \sigma_{ast}^2 + \sigma_{track}^2\right)} \\ \sigma_{bq}^2 = 4\sigma_s^2 \\ \sigma_{ast} = \sqrt{\dfrac{H_t^2 + W_S^2}{8d_{HR}}} \\ H_t = \sqrt{LW \times LH}\left|\dfrac{d_{HR}}{f} - \cos\theta\right| \\ W_S = \sqrt{LW \times LH}\left|\dfrac{d_{HR}}{f}\cos\theta - 1\right| \end{cases} \tag{26}$$

2.3.7 Fixed heliostat field output thermal power

The formula for the output thermal power E_{field} for the fixed heliostat field is derived from solving the fixed heliostat field model:

$$\begin{cases} \eta = \eta_{sb}\eta_{\cos}\eta_{at}\eta_{trunc}\eta_{ref} \\ E_{field} = DNI \cdot \sum_i^N A_i\eta_i \\ A_i = LW_i \times LH_i \end{cases} \tag{27}$$

3. Parametric Optimization of Heliostat Fields

The optimization model for the heliostat field parameters was developed based on the established heliostat field model, with the primary goal of achieving a rated power of 60*MV*. According to literature, in similar conditions in the northern hemisphere, such as in a power plant in Spain, optimal positioning of the absorption tower within the heliostat field requires a shift towards the negative direction of the y-axis, corresponding to the positive south direction. This specific positioning is essential for maximizing the annual average thermal power output per unit area, as indicated by theoretical findings from the literature[8]. To simplify the calculation process within the optimization model, the Campo arrangement method is employed for the placement of heliostats in the field[9-10]. This method, which results in a dense heliostat field and imposes certain sacrifices in shadow shading efficiency, is found to be instrumental in achieving the optimum annual average thermal power output. Subsequently, a schematic diagram illustrating the heliostat arrangement is developed based on this arrangement method.

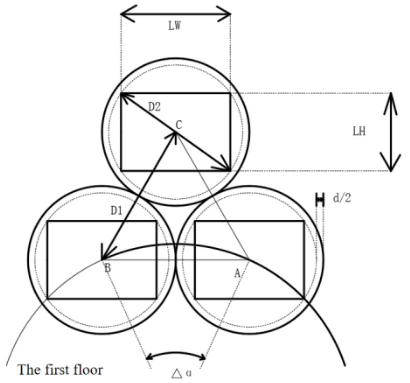

Figure 4 Schematic diagram of heliostat placement

Schematic analysis of heliostat placement, D_1 in the figure 4 from the first layer to start calculating, to extend outward to achieve a dense heliostat field, based on the topic given the requirements of adjacent heliostat base center distance than the mirror width LW at least 5*m*, then the following expression:

$$D_1 \geq LW + 5 \tag{28}$$

The analysis shows that the smaller the distance D_1 is, the more number of heliostats are accommodated in the heliostat field, and the optimization is better. Therefore Eq.(28) can be transformed into:

$$D_1 = LW + 5 \tag{29}$$

The optimization model is obtained as follows:

objective function: $\max\ E_{year}$

$$\text{restrictive condition：}\ s.t.\begin{cases} 2 \leq LH \leq LW \leq 8 \\ 2 \leq z \leq 6\ ,\ z \geq \dfrac{LH}{2} \\ D_1 = LW + 5 \\ {x_i}^2 + (y_i - y_0)^2 \geq 100^2 \\ {x_i}^2 + y_i^2 \leq 350^2\ ,\ y_0 \leq 350 \\ E_{fieldyear} \geq 6 \times 10^4 \end{cases} \tag{30}$$

Careful consideration of the optimization parameters is crucial to effectively tackle the challenges posed by the high dimensionality, large overall size, and complex environment of this optimization model. Given the model's characteristics, the application of a genetic algorithm is a more appropriate approach for solving this optimization model, as it is better suited for handling the associated complexities. This is in contrast to using a traditional optimization algorithm, which may lead to prolonged computation time and susceptibility to converging to a local optimum. As a result, the solution's outcomes are depicted in figure 5.

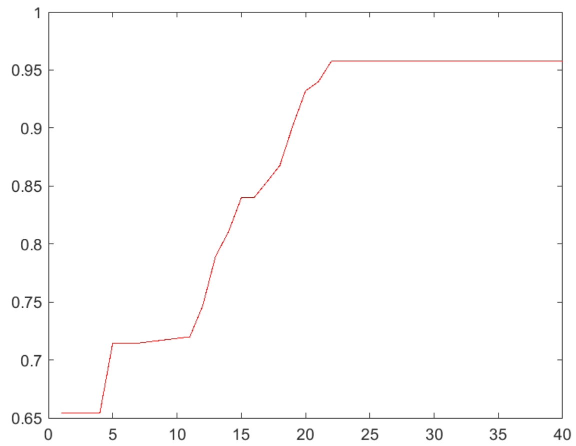

Figure 5 Genetic Image

Analysis of the genetic image shows that the function value, i.e., the average annual output thermal power per unit area of the mirror, tends to be stable after the 22nd generation of inheritance, converging at 0.9575kW/m^2, and the results of the optimization model solution in this context are obtained in Table 1, 2 and 3.

Table 1 Average optical efficiency and output power on the 21st of each month

Dates	Average optical efficiency	Average cosine efficiency	Average Shadow Occlusion Efficiency	Average truncation efficiency	Average thermal power output per unit area of mirror(kW/m^2)
1.21	0.5013	0.7798	0.8528	0.9788	1.1008
2.21	0.4926	0.7384	0.9209	0.8367	0.7991
3.21	0.4893	0.7805	0.9163	0.8078	1.1412
4.21	0.4755	0.7377	0.9182	0.8356	1.0035
5.21	0.4463	0.6378	0.9327	0.8976	0.7264
6.21	0.5673	0.7515	0.8728	0.9677	1.0709
7.21	0.5307	0.6171	0.8476	0.9895	0.7695
8.21	0.5188	0.7156	0.926	0.8427	0.983
9.21	0.4573	0.6740	0.9044	0.8561	1.2297
10.21	0.4496	0.6452	0.9341	0.8078	0.7009
11.21	0.5266	0.6657	0.8524	0.9825	0.9892
12.21	0.5565	0.7960	0.8429	0.9765	0.8979

Table 2 Annual average optical efficiency and output power table

Annual average optical efficiency	Annual average cosine efficiency	Annual average shadow shading efficiency	Annual average truncation efficiency	Annual average thermal power output (MW)	Annual average thermal power output per unit area of mirror(kW/m^2)
0.5010	0.7112	0.8934	0.9169	60.1332	0.9575

Table 3 Design parameters of the heliostat field

Absorption tower position coordinates	Size of Fixed Sun Mirror ($W \times H$)	Installation height of heliostat (m)	Total number of heliostats	Total area of fixation mirrors (m^2)
(0, -87.5656)	4.7825×4.3666	3.1332	3010	62858.62615

4. Conclusions

The development of a sophisticated research framework aiming to enhance heliostat field design optimization for sustainable energy solutions is the central focus of this paper. This research framework holds significant importance for advancing the efficiency and effectiveness of sustainable energy solutions.The optimized design has yielded an impressive output of 0.9575MW/m^2. The comprehensive calculations included key determinants such as the location coordinates of the absorption tower, dimensions and installation height of the heliostat mirrors, and the precise determination of the total number of mirrors, which was found to be 3010. To enhance output efficiency, the Campo arrangement method was meticulously employed to organize the heliostats in circular fields.

The integration of genetic algorithms in this multi-model approach has not only proven effective in optimizing the structural and efficiency aspects of heliostat fields but also validates the model's accuracy and applicability. This methodology provides a comprehensive and efficient framework for designing heliostat fields, potentially influencing future developments in solar energy harnessing. The findings of this study serve as a valuable reference for optimizing heliostat field design and offer insights that could spearhead further research in sustainable energy technologies.

References

[1] Zhuang Yanhao. Derivation of solar altitude angle and solar azimuth angle formulas based on subject integration - An example of senior three geography test questions in ten schools in Jinhua in November 2020[J]. Geography Teaching, 2022(02): 38-40.

[2] Cooper P.I.The absorption of radiation in solar stills[J].Solar Energy,1969,12(3):333-346.

[3] Du Yuhang et al, Impact analysis of different focusing strategies of heliostats in tower-type photovoltaic power plants[J], Journal of Power Engineering, 2020, 40(5):426-432.

[4] FANG Miaosen, LU Jing, SHEN Zhigang. Modeling of front-end efficiency of tower solar heliostat and its application[J]. Journal of Changzhou Institute of Information Technology,2021,20(03):20-24.

[5] O. Farges, J.J. Bezian, M. El Hafi, Global optimization of solar power tower systems using a Monte Car lo algorithm: Application to a redesign of the PS10 solar thermal power plant [J], Renewable Energy, 20 18, 119:345-353.

[6] HUANG Ju, YAN Zhiguo, DENG Biao et al. Current status of research on mirror field design software for tower solar thermal power plants[J]. Oriental Electric Review,2023,37(02):41-47.DOI:10.13661/j.cnki.issn1001-9006.2023.02.014.

[7] WEN Long, XIAO Bin, ZHOU Zhi, et al. Simulation analysis of heliostat imaging based on HFLCAL computational model[J]. Solar Energy,2017(07):46-49.DOI:10.19911/j.1003-0417.2017.07.008.

[8] Liu Jianxing. Optical efficiency modeling simulation and optimal arrangement of heliostat mirror field for tower-type photovoltaic power plant[D]. Lanzhou Jiaotong University,2022.DOI:10.27205/d.cnki.gltec.2022.001089.

[9] Chao L, Zhai R, et al.Optimization of a heliostat field layout using hybrid PSO-GA algorithm[J].Applied Thermal Engineering,2018,128(06):23-35

[10] GAO Bo, LIU Jianxing, SUN Hao, et al. Optimal arrangement of heliostat mirror field based on adaptive gravitational search algorithm[J]. Journal of Solar Energy,2022,43(10):119-125.DOI:10.19912/j.0254-0096.tynxb.2021-0397